Nanoscale

PAPER

View Article Online
View Journal | View Issue

Cite this: *Nanoscale*, 2014, **6**, 11921

Emission tunable, cyto/hemocompatible, near-IR-emitting Ag_2S quantum dots by aqueous decomposition of DMSA†

Ibrahim Hocaoglu,[a] Fatma Demir,[a] Ozgur Birer,[abc] Alper Kiraz,[ad] Chantal Sevrin,[e] Christian Grandfils[e] and Havva Yagci Acar*[abc]

Received 28th May 2014
Accepted 31st July 2014

DOI: 10.1039/c4nr02935f

www.rsc.org/nanoscale

Size tunable aqueous Ag_2S quantum dots emitting in the near-infrared region were synthesized through decomposition of *meso*-2,3-dimercaptosuccinic acid (DMSA) in water. The resulting NIR QDs are highly cyto- and hemocompatible, have quantum yields as high as 6.5% and are effective optical imaging agents based on *in vitro* evaluation.

Introduction

Size and emission tunability, broad absorption and narrow emission properties of quantum dots (QDs) have attracted a great deal of attention to enable a variety of technological developments. QDs can be used in electronics, optics, energy and biomedical applications due to their versatile properties. Cadmium-based semiconductor nanoparticles (CdX, X: S, Se, Te) are the most widely studied quantum dots emitting in the visible region (400–700 nm). Unfortunately, emission in the visible region is not practical for biological applications such as imaging/diagnostics.

Quantum dots emitting in the near-infrared region (NIRQDs) have emerged in response to the increasing demand for more suitable QDs in biotechnology and medicine. Biological molecules or natural constituents such as hemoglobin, deoxyhemoglobin and water have intense interactions with visible monochromatic light.[1] Living tissues also have autofluorescence in the visible region. The near-infrared (NIR) region between 700 and 900 nm where absorption and scattering activities are lower in living tissues is defined as the therapeutic window.[1,2]

The most frequently used NIRQDs are Cd-based, such as CdTeS, CdHgTe/CdS[3] and CdSe/CdTe,[4] and there are a few examples of their bio-applications.[5,6] For example, Prasad *et al.* showed imaging of panc-1-tumor using functionalized CdTe/ZnS QDs.[7] CdMnTe/Hg QDs were used as angiographic contrast agents by Morgan *et al.*[8] and CdTe/CdS QDs were used in *in vitro* cell and *in vivo* tumor imaging.[9] However, heavy metal toxicity is an important concern for both *in vitro* and *in vivo* studies.[10] Recent efforts are directed towards the development of Cd, Pb and Hg free, biocompatible QDs. From this perspective, silver chalcogenide quantum dots with a band gap of 0.9 eV and superior biocompatibility over Cd-based QDs are excellent candidates for bio-applications. There are two recent studies on the evaluation of cytotoxicity, cell proliferation, ROS generation, apoptosis, necrosis and DNA damage of Ag_2S QDs and both of them reported high biocompatibility.[11,12]

Most of the Ag_2X (X: S, Se, Te) NIRQDs in the literature have been prepared in an organic medium using organic soluble coating materials.[13–16] Those quantum dots have emission characteristics in the 650–1200 nm range with very low photoluminescence quantum yield (below 2%).[15,16] Alternatively, Zhu *et al.* synthesized Ag_2S nanoparticles in ethyleneglycol at above 140 °C by the decomposition of 3-mercaptopropionic acid and transferred the resulting particles into a water phase without any ligand exchange procedure.[17]

There are also a few examples of Ag_2S NIRQDs prepared in aqueous media. Remya *et al.* prepared aqueous Ag_2S nanoclusters in two steps through hydrothermal decomposition of the glutathione complex of Ag nanoparticles at low temperature over 24 h.[18] Castañon *et al.* reported aqueous synthesis of Ag_2S nanoparticles larger than 30 nm without any emission data.[19] Hocaoglu *et al.* have recently demonstrated a simpler, single-step synthesis of cytocompatible Ag_2S–2MPA NIRQDs *via* direct addition of a sulphur source to a silver salt in water.[20] These NIRQDs have high QYs compared to those reported in the literature but failed to produce particles luminescing at significantly different wavelengths along with good QY. A common approach towards manipulating size is the adjustment of

[a]*Koc University, Graduate School of Materials Science and Engineering, Rumelifeneri Yolu, Sarıyer, 34450, Istanbul, Turkey. E-mail: fyagci@ku.edu.tr; Fax: +90-2123381559; Tel: +90-2123381742*

[b]*Koc University, Department of Chemistry, Rumelifeneri Yolu, Sarıyer, 34450, Istanbul, Turkey*

[c]*KUYTAM, Koc University Surface Science and Technology Center, Rumelifeneri Yolu, Sarıyer, 34450, Istanbul, Turkey*

[d]*Koc University, Department of Physics, Rumelifeneri Yolu, Sarıyer, 34450, Istanbul, Turkey*

[e]*Centre Interfacultaire des Biomatériaux (CEIB), University of Liège (ULg), Chemistry Institute, B6c, Allée du 6 août, 11, B-4000 Liège (Sart-Tilman), Belgium*

† Electronic supplementary information (ESI) available. See DOI: 10.1039/c4nr02935f

reaction time, ligand/Ag or Ag/S ratio which usually failed in the case of Ag_2S.[12,20] Recently, Yang *et al.* reported Ag_2S–BSA QDs with emission between 1050–1295 nm through Ag/S ratio variation.[21] Glutathione stabilized Ag_2S QDs were prepared (960–1050 nm) with 0.96–1.97% QY (reference: indocyanine green, QY 13%).[22] Most recently, Gui *et al.* reported size tunable (687–1096 nm) Ag_2S QDs prepared with poly(acrylic acid)-*graft*-cysteamine-*graft*-ethylenediamine coating with QY 14–16% (reference: indocyanine green).[23]

We have previously demonstrated that *meso*-2,3-dimercaptosuccinic acid (DMSA) can be used as a slow sulphur releasing agent between pH 7 and 10 and at temperatures between 50 and 90 °C.[24] Size tunable CdS QDs were synthesized by the decomposition of DMSA and the best condition for effective size tuning was determined as pH 7.5 and 70 °C.[24] In such reactions, DMSA acted both as a sulphur source and a coating material. Furthermore, DMSA is a metal chelating agent[25] and an FDA approved drug used in heavy metal poisoning.[26] DMSA coating improved the cytocompatibility of CdS QDs significantly.

In this article, DMSA is evaluated as a slow S-releasing reagent and a biocompatible coating material in an effort to synthesize biocompatible, size tunable Ag_2S NIR QDs in a very simple procedure. At molar ratios of DMSA/Ag of 1.5, 2.5 and 3.5 particles with emission maximum between 730–860 nm with QYs as high as 6.5% were achieved at 70 °C within 5 h. *In vitro* assessment of cytocompatibility and hemocompatibility tests were performed for these Ag_2S/DMSA NIRQDs. The cytotoxicity of QDs is frequently determined, however, until now, very few studies have examined the hemocompatibility of QDs.[27–29] Indeed, when diluted in the blood stream, nanomaterials will be able to elicit several toxicological reactions, in particular embolisation, hemolysis, and cellular activation, but also several well-known biological cascades such as coagulation, complement activation, kinin/kininogen, and fibrinolysis. Moreover, it is important to stress that the first barrier that nanoparticles encounter is the blood itself and the Reticulo-Endothelial System (RES). Because of the high efficiency of this clearance system in eliminating foreign bodies from the blood circulation, the blood life-time of nanoparticles does not typically exceed seconds/minutes. Therefore, in addition to cytocompatibility, assessment of hemocompatibility is essential before considering any preclinical studies. Compared to macroscopic particles, the hemoreactivity of nanoparticles may be expected to be significantly enhanced due to a very high surface/volume ratio. Therefore, a significant interaction of nanoparticles with humoral and cellular blood components of the blood is highly expected.

These Ag_2S/DMSA NIRQDs are non-toxic up to 200 μg mL^{-1} in HeLa cancer cell lines and showed only 20% reduction in cell viability of 3T3 NIH cells in 24 h. Hemocompatibility testing has also highlighted that they do not elicit any major reaction within the blood up to a concentration of 100 μg mL^{-1}. They have provided efficient cytoplasmic labelling of HeLa cells demonstrating great ability for optical imaging.

Materials and methods

Materials

All reagents were of analytical grade or highest purity. *meso*-2,3-Dimercaptosuccinic acid (DMSA) and silver nitrate ($AgNO_3$) were purchased from Sigma-Aldrich. Sodium sulfide (Na_2S) was purchased from Alfa-Aesar. Sodium hydroxide (NaOH), 2-mercaptopropionic acid (2-MPA), ethanol and acetic acid (CH_3COOH) were purchased from Merck. LDS 798 Near-IR laser dye was purchased from Exciton Inc. Only Milli-Q water (18.2 MOhm) was used when needed. For biological applications, DMEM (with 4500 mg L^{-1} glucose, 4.0 mM L-glutamine, and 110 mg L^{-1} sodium pyruvate), trypsin–EDTA, penicillin–streptomycin and fetal bovine serum were purchased from HyClone, USA. Thiazolyl blue tetrazolium bromide (MTT) *Biochemica* was purchased from AppliChem, Germany. Paraformaldehyde solution 4% in PBS and UltraCruz™ 96 well plates were purchased from Santa Cruz Biotechnology, Inc., USA. Glass bottom dishes were purchased from MadTek, USA. Dimethyl sulfoxide Hybri-Max™ and phosphate buffered saline (pH 7.4) were purchased from Sigma, USA.

Preparation of Ag_2S nanoparticles

As an example, 42.5 mg of $AgNO_3$ was dissolved in 75 mL of deoxygenated deionized water. 25 mL of deoxygenated aqueous DMSA solution prepared at pH 7.5 was then added to the reaction mixture. The pH of the solution was adjusted to 7.5 by using NaOH and CH_3COOH solutions (2 M). Under vigorous mechanical stirring at 5000 rpm, the reaction mixture was brought to the desired temperature (70 or 90 °C). During the reaction, samples were taken at different time points to follow the particle growth. The prepared quantum dot solutions were washed with DI water using Amicon-Ultra centrifugal filters (3000 Da cut off) and stored in the dark at 4 °C.

The influence of reaction variables was studied in different reactions keeping the Ag concentration fixed at 2.5 mM and varying the DMSA concentration to achieve DMSA/Ag ratios of 1.5, 2.5 and 3.5 (Tables 1 and 2).

Cell culture

Human cervical carcinoma (HeLa) and mouse fibroblast cells (NIH-3T3) were cultured according to ATCC recommendations. Cells were cultured in DMEM with 4500 mg L^{-1} glucose, 4.0 mM L-glutamine, and 110 mg L^{-1} sodium pyruvate. Complete medium also contained 10% fetal bovine serum and 1% penicillin–streptomycin antibiotic solution. Trypsin–EDTA was used for cell detachment and cells were incubated at 37 °C under 5% CO_2.

Determination of cytotoxicity

Cytotoxicity was evaluated by performing the thiazolyl blue tetrazolium bromide (3-(4,5-dimethyl-thiazol-2yl)-2,5-diphenyltetrazolium bromide, MTT) assay on HeLa and NIH-3T3 cells. 96-well culture plates were seeded with 10^4 cells in culture medium and incubated at 37 °C and 5% CO_2 for 24 h. Following

Table 1 Influence of the DMSA/Ag ratio and reaction time on the properties of Ag_2S–DMSA NIRQDs[a]

DMSA/Ag	Time	λ_{cutoff}[b] (nm)	Size[c] (nm)	Band gap (eV)	$\lambda_{em,max}$ (nm)	FWHM (nm)	QY[d] (%)
1.5	1 h	662	2.20	1.88	782	195	
1.5	3 h	792	2.57	1.57	800	173	
1.5	4 h	844	2.73	1.47	828	158	
1.5	5 h	870	2.82	1.43	858	150	
1.5	19 h	907	2.95	1.37	923	—	
2.5	1 h	677	2.24	1.83	730	170	
2.5	3 h	791	2.60	1.57	789	129	
2.5	4 h	810	2.62	1.53	810	139	6.5
2.5	5 h	833	2.70	1.49	829	137	6.3
3.5	30 min	625	2.10	1.99	730	—	
3.5	2 h	807	2.61	1.54	794	142	
3.5	4 h	837	2.71	1.48	834	134	6.4
3.5	9 h	890	2.89	1.40	910	>180	

[a] $T = 70$ °C, pH = 7.5. [b] Determined from the absorbance spectrum. [c] Diameters of the particles calculated by the Brus equation. [d] Quantum yield. LDS 798 NIR dye was used as a reference.

Table 2 Influence of the temperature on DMSA decomposition and NIRQD properties[a]

Time (min)	λ_{cutoff}[b] (nm)	Size[c] (nm)	Band gap (eV)	$\lambda_{em,max}$ (nm)	FWHM (nm)
30	739	2.41	1.68	760	150
60	837	2.70	1.48	840	165
90	886	2.87	1.40	875	168
120	886	2.87	1.40	926	>170

[a] T = 90 °C, DMSA/Ag = 2.5. [b] Determined from the absorbance spectrum. [c] Diameters of the particles calculated by the Brus equation.

incubation, the medium was replenished; cells were treated with QDs (10 to 150 μg mL^{-1} Ag) and incubated for 24 h. After washing, MTT reaction solution was added to the cells and incubated for 4 h. DMSO–ethanol (1 : 1) solution (100 μL) was added with gentle shaking for 15 min to dissolve the purple formazan. The absorbance at 600 and 630 nm was measured with an ELISA analyzer and the reference absorbance at 630 nm was subtracted from the absorbance at 600 nm. Experiments were repeated four times. Absorbance values of the QDs were subtracted from the formazan values. The statistical significance of the observed differences was determined using one-way ANOVA with Tukey's multiple comparison test of GraphPad Prism software package from GraphPad Software, Inc., USA.

Cell imaging

50 000 HeLa cells were seeded in glass bottom dishes. After 18 h incubation, cells were treated with 150 μg mL^{-1} QDs in full medium for 6 h. After being washed with PBS (pH 7.4), cells were fixed with 4% paraformaldehyde for 15 min and the wash step was repeated.

A home-built sample scanning confocal microscope based on an inverted microscope frame (Nikon TE 2000U) equipped with a 60× (Nikon, NA = 1.49) oil immersion objective was used for image acquisition. The excitation wavelength was 532 nm. A broadband 10/90 dichroic beam splitter was used for excitation. A long pass glass filter (RG665) was placed before silicon APD based photon counting modules to detect the QD emission.

Hemocompatibility studies

Hemocompatibility tests were performed with Ag_2S NIRQDs which were synthesized at a DMSA/Ag ratio of 2.5, 70 °C in 4 h. Hemocompatibility tests were performed according to ISO standards (10993-4). Normal human blood from healthy volunteer donors was collected in Terumo Venosafe citrated tubes (Terumo Europe N. V., Belgium). Experiments were done within 2 h after blood collection. All tests were performed with the agreement of the local ethical committee of the Medicine Faculty of the University of Liège. The hemocompatibility of Ag_2S/DMSA NIRQDs was evaluated by studying hemolysis, the morphology of blood cells, complement activation (C3a), and coagulation activation, both through the extrinsic pathway (PT assay) and the intrinsic pathway (APTT assay). QDs dispersed in PBS were diluted in whole blood in order to obtain the final nanoparticle concentrations of 100, 10, and 1 μg mL^{-1}. Samples were incubated for 15 min at 37 °C under lateral agitation (250 rpm).

Micrographs of blood smear

After blood incubation, 5 μL of the blood was withdrawn and spread on a microscopy glass slide. Blood cells were observed with an Olympus Provis microscope at 20× and 50× magnification in transmission mode.

Haemolysis

The haemolytic test was performed following Standard Practice for Assessment of Haemolytic Properties of Materials (ASTM designation F 756-00). Briefly, after QD incubation in whole blood, the samples were centrifuged at 600*g* for 5 min at room temperature, and supernatants were collected and mixed with the cyanmethemoglobin reagent. The hemoglobin released was measured by reading the absorbance of 100-fold dilution of

whole blood in Drabkin's reagent at 540 nm in a microplate reader (Anthos HT III, type 12600, Anthos, Salzburg, AU). A calibration curve was established using bovine hemoglobin as the standard. Saponine (0.8 mg mL^{-1}) and PBS were used as positive and negative controls, respectively. Hemolysis was expressed as the percentage of hemoglobin released to the total hemoglobin content, taking the positive control as 100% of hemolysis. The tests were done in triplicate.

Count and size distribution of RBCs, platelets and white blood cells

QD dispersions and blood were prepared and incubated as described before. After 15 min of incubation, blood cells were counted and their size distribution was determined with CELL-DYN 18 Emerald (Abbott Diagnostics). Three analyses were conducted per sample.

Complement activation

Complement activation was assessed using the Human C3a ELISA kit for quantification of Human C3a-des-Arg (Becton Dickinson). After a 15 min incubation of blood and QD mixtures, EDTA (1 mM final) was added to block any future complement activation. Samples were centrifuged at 2000*g* for 5 min at rt, and supernatants were used for the analysis of complement activation following the kit protocol (BD OptEIA, Human C3a ELISA, Cat. no. 550499). Absorbance was measured at 450 nm with a microplate reader (Anthos HT III, type 12600). Plasma containing 2 mg mL^{-1} of Zymosan was taken as a positive control and plasma without additives as a negative control. The concentration of C3a was expressed as a percentage of activation by reference to the negative control set at a value of 100% of complement activation. Measurements were done in duplicate.

Coagulation experiments

Whole blood and QD dispersions were mixed and incubated as described before. Samples were centrifuged at 2000*g* for 5 min at rt, and the supernatants were collected, recalcified to reverse the effect of the citrate anticoagulant, and supplied with the specific activators of coagulation (thromboplastin). The prothrombin time (PT) to evaluate the extrinsic pathway and the activated partial thromboplastin time (APTT) to evaluate the intrinsic pathway were measured directly with a Dade Behring Coagulation Timer analyzer (BCT) (Siemens Healthcare Diagnostics NV/SA, Belgium) using commercial reagents (Thromborel® S, Dade Behring/Siemens, for PT determination and C.K. PREST kit, Roche Diagnostics, France, for APTT). Kaolin reagent was used as a positive control and PBS as a negative control. The clotting time was measured for each sample, and the coagulation capacity was expressed as a percentage, taking the value of standard human plasma (Dade Behring/Siemens) as 100%. Measurements were done in duplicate.

Characterization methods

A Shimadzu 3101 PC UV-vis-NIR spectrometer was utilized for absorbance spectroscopy in the 300–1000 nm range. The Brus equation[30,31] (eqn (1)) was used for the particle size calculation from the experimentally determined absorption onset.

$$\Delta E = \frac{\hbar^2\pi^2}{8R^2}\left[\frac{1}{m_e}+\frac{1}{m_h}\right] - 1.8\frac{e^2}{\varepsilon_{Ag_2S}4\pi\varepsilon_0 R} \quad (1)$$

ΔE is the band gap energy difference between the bulk semiconductor and the quantum dot, R is the radius of the quantum dot, m_e ($0.286m_0$) and m_h (1.096) are the respective effective electron and hole masses for Ag_2S,[32] and ε_{Ag_2S} (5.95) is the dielectric constant of bulk Ag_2S.[32]

Photoluminescence spectra were recorded with a homemade setup. The system was built around a 1/8 monochromator (Newport Cornerstone 130) equipped with a 600 L per mm grating working in the 400–1000 nm range. The excitation source was the frequency doubled output of a DPSS laser at 532 nm. The luminescence signal was filtered using a 590 nm long pass filter before it was wavelength selected and detected with a Si detector with femtowatt sensitivity (Thorlabs PDF10A, 1.4×10^{-15} W $Hz^{-1/2}$). The power of the excitation source was monitored with a powermeter and the reported spectra were normalized for excitation power.

QY calculations were done based on the procedures detailed in the literature.[33–35] As a reference LDS 798 NIR dye (QY = 14%, reported by the producer) was used. Typically, five different concentrations of the dye (in MeOH) and sample (in water) were prepared, all with absorption below 0.15 at excitation wavelength and the PL spectra of each were obtained. The proportion of the areas under the emission peaks was used in the calculations. Area values of the different concentrations were plotted for both samples and the reference dye (standard). The typical QY is the ratio of the slope of the sample (m_{slope}) and the slope of the dye ($m_{standard}$). The equation below is used for QY calculation (eqn (2)).

$$\Phi_{yield} = \frac{m_{sample}}{m_{standard}}\left(\frac{{\eta_{water}}^2}{{\eta_{MeOH}}^2}\right) \quad (2)$$

Refractive indices of the sample (η_{water}) and the reference dye (η_{MeOH}) solutions are important for the calculation.

Samples were dried into powder form using a freeze-drier for X-PS and XRD analysis. XPS analyses were performed with a Thermo Scientific K-Alpha XPS with Al K-alpha monochromatic radiation (1486.3 eV). Ag_2S powders were placed on adhesive aluminum tape and 400 μm X-ray spot size was used. The pass energy of 50.0 eV corresponds to a resolution of roughly 0.5 eV. The base pressure was below 3×10^{-9} mbar and the experimental pressure was about 1×10^{-7} mbar due to charge neutralization with a flood gun. The C1s peak at 285.0 eV was assigned as the reference signal for evaluation.

A D8 advance Bruker instrument was used for the XRD. Solid samples were put on a piece of glass with double sided tape. The glass was placed into the sample holder with dough. Crystal peaks were recorded between 2θ angles of 10–80° with Cu Kα radiation ($\lambda = 1.5406$).

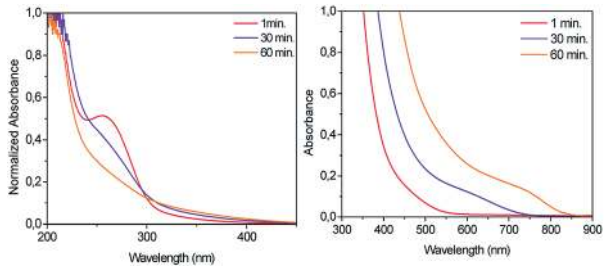

Fig. 1 Absorbance spectra of Ag^+–DMSA complex (left) and Ag_2S–DMSA (right) NIRQDs prepared at 90 °C at DMSA/Ag = 2.5.

For TEM analysis, a JEOL ARM 200 CFEG Cs-corrected STEM operating at 200 kV was used. EDS was done with a JEOL Centurion detector with 100 mm^2 detector area.

The hydrodynamic size and the zeta potential of the aqueous colloidal Ag_2S/DMSA were measured using a Malvern zetasizer nano ZS.

The Ag^+ ion concentration of the quantum dot solutions was determined using a Spectro Genesis FEE Inductively Coupled Plasma Optical Emission Spectrometer (ICP OES) using appropriate regression curves created with standard solutions. QDs were etched with a nitric acid and sulfuric acid mixture and diluted with DI water for the ICP analysis. Experiments were done in triplicate and the average was reported.

Results and discussion

In a typical reaction, Ag^+ and DMSA form a complex with a strong absorbance at around 255 nm (Fig. 1a). The absorbance maximum of the initial complex vanishes slowly with time as the reaction mixture was heated indicating the decomposition of the complex and formation of the Ag_2S crystals. As Ag_2S nanocrystals form and grow, the absorbance onset shifts to longer wavelengths (Fig. 1b).

The primary purpose of using DMSA here is to benefit from slow sulphur release from DMSA to tune the crystal size and therefore the emission wavelength of Ag_2S QDs. Therefore, the DMSA/Ag ratio and the reaction temperature which influence the decomposition rate were studied as variables and their

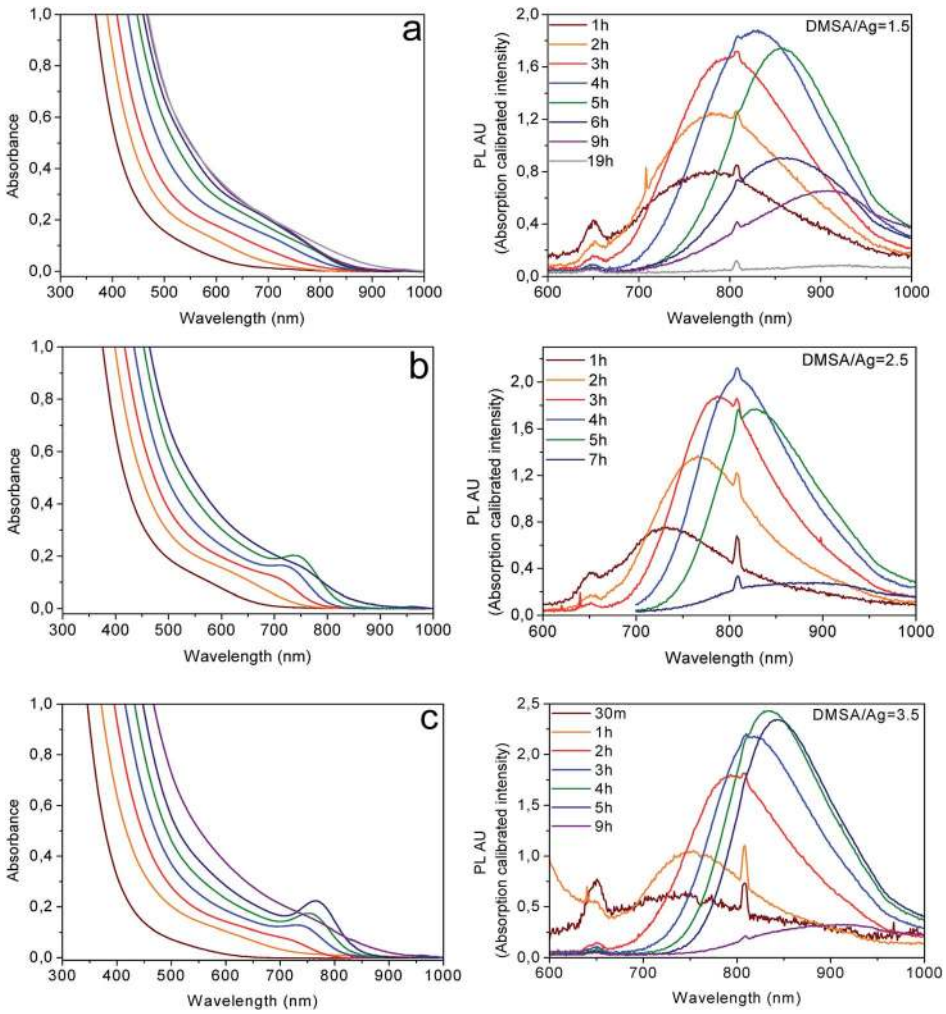

Fig. 2 Absorbance and corresponding photoluminescence spectra of Ag_2S–DMSA NIRQDs at different time points during the synthesis performed at 70 °C and DMSA/Ag ratios of (a) 1.5, (b) 2.5 and (c) 3.5.

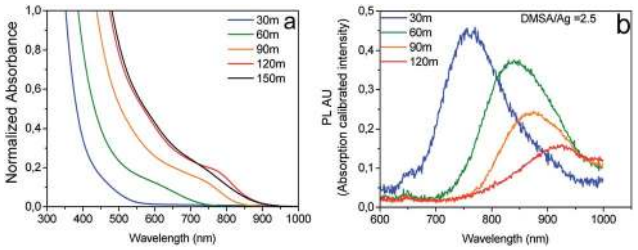

Fig. 3 Absorbance (a) and PL (b) spectra of the samples taken from the synthesis of Ag_2S NIRQDs at 90 °C.

influence on the particle size, emission wavelength and quantum yield was analysed. Three different DMSA/Ag ratios were used at a fixed temperature of 70 °C and pH 7.5.

The initial reaction at a DMSA/Ag ratio of 1.5 was monitored for 19 h using a UV-vis spectrophotometer and spectrofluorometer (Fig. 2a). The red shift of the absorbance onset implies crystal growth with time as DMSA decomposes slowly and releases sulphur. This profile is completely different from those obtained with 2MPA coating and Na_2S as a sulphur source, where only the intensity changed with time. Crystal sizes of Ag_2S/DMSA QDs increased from 2.20 to 2.95 nm with time as calculated by the Brus equation using the absorbance onsets (Table 1). The increase in crystal sizes was accompanied by the red shift in emission maximum of the particles from *ca.* 780 to 920 nm. The luminescence intensity of the particles continuously increased up to 4 h (emission maximum at 828 nm) and then decreased with further increase in particle size. A major drop in the luminescence intensity was observed at the 5th h.

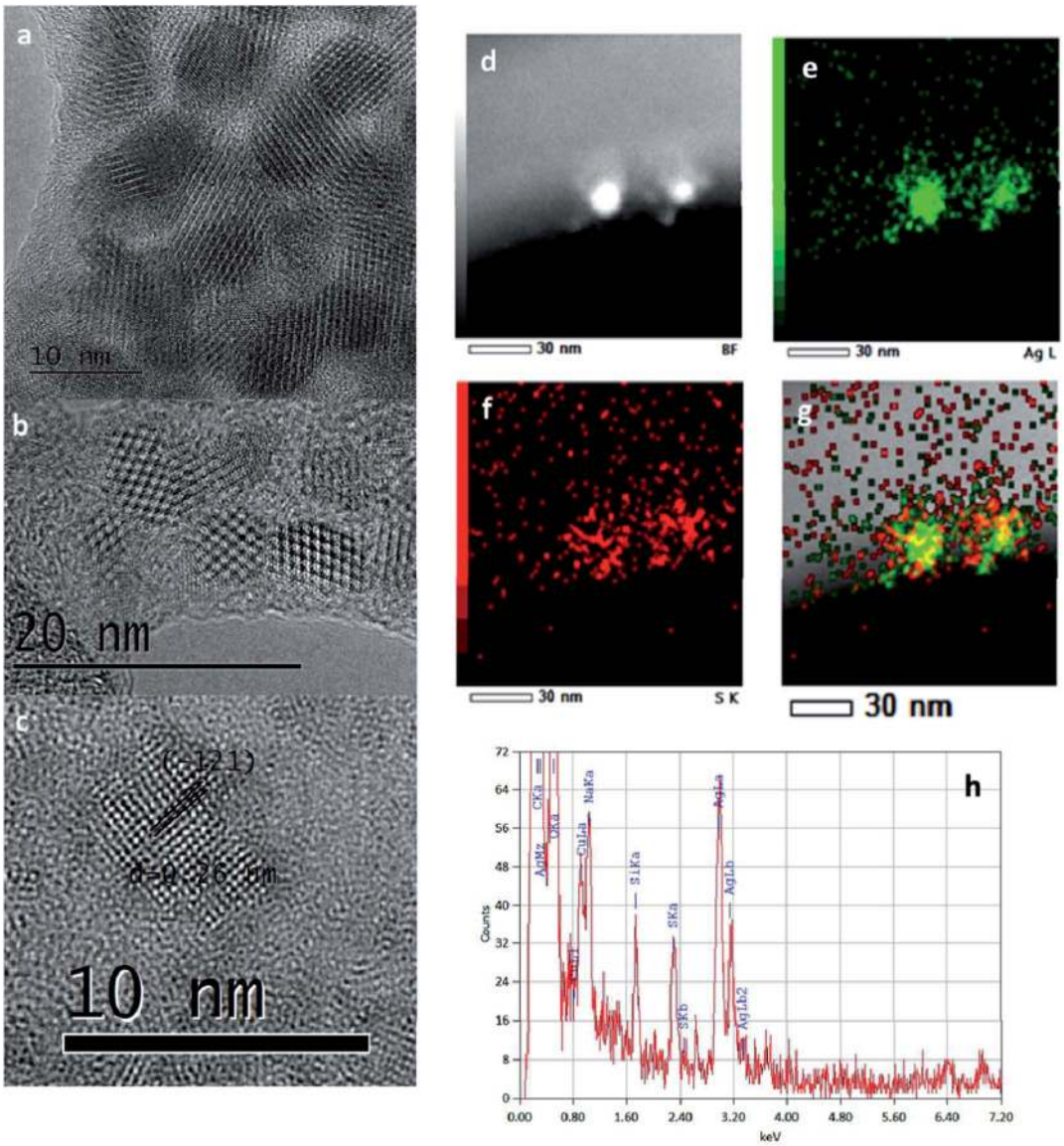

Fig. 4 TEM and EDX analyses of the Ag_2S–DMSA NIRQDs. TEM images of the nanoparticles at (a) 10 nm and (b) 20 nm scales, (c) focused lattice planes for defining the *d*-spacing parameter corresponding plane. (d) Bright field image of the Ag_2S–DMSA NIRQDs, (e) Ag and (f) S elemental mapping and (g) their merged image showing the composition of the particles. (h) Ag and S transitions by EDX acquisition.

Yet, DMSA decomposition provided size tunable Ag_2S NIRQDs luminescing between 780 and 920 nm in a one pot reaction.

Reactions were performed at higher DMSA/Ag ratio as well to evaluate its impact on the rate of crystal growth, size tunability and luminescence efficiency. Increasing the DMSA amount impacts the reaction in two counteracting ways: larger amounts of DMSA can reduce the particle size as it can passify the surface of the growing crystals at an earlier stage. On the other hand, increasing the DMSA amount introduces more S^{2-} to the medium through decomposition which decreases the Ag/S ratio and increases the particle size. Absorbance and photoluminescence spectra of Ag_2S synthesized at a DMSA/Ag ratio of 2.5 and 3.5 are shown in Fig. 2b and c. As particles grow with time, a distinctive absorption feature appeared in 3 h and luminescence maxima starting around 750 nm shifted towards 850 nm in 5 h. Any further reaction caused a dramatic drop in the luminescence intensity although the emission maximum shifted to *ca.* 920 nm. As the DMSA/Ag ratio increased the major impact was seen in the full width at half maximum (FWHM) as it got narrower at high ratios. Increasing the DMSA amount from 1.5 to 2.5 caused a small decrease in size and a slight blue shift in the emission peak and increasing further to 3.5 increased the size and caused a slight red shift in the emission (Fig. S1†). These refer to early passivation of the growing crystal with increasing coating amount, and increasing crystal size with decreasing Ag/S ratio at higher concentration of DMSA, as proposed previously. But overall, increasing the DMSA/Ag ratio did not cause a dramatic increase in particle size/emission maximum but a narrowing in the emission peak with a slight increase in luminescence intensity at a ratio of 3.5 (Fig. S1 and Table S1†). These indicate that at these ratios (2.5 and 3.5) excess DMSA was most influential in stabilizing the surface. At all DMSA/Ag ratios QDs produced in 4 h have the highest luminescence intensity within the 810–834 nm peak emission range with a QY around 6.4% with respect to LDS 798 NIR dye (14% QY in DMSO) (Tables 1 and S1†) which is quite good compared to most NIR emitting QDs in the literature[21] and good enough to evaluate these particles for bio-imaging purposes as will be demonstrated later in this article.

One of the important parameters affecting decomposition of DMSA and particle growth is temperature. Synthesis of Ag_2S–DMSA NIRQDs (DMSA/Ag = 2.5) at 90 °C speeded up the sulphur release and the crystal growth. As can be seen in the absorbance spectra in Fig. 3a, particle growth stopped at the 3rd hour.

A distinct red shift in emission maximum was observed every 30 min from 750 to 900 nm. Particles with emission maximum at 830–840 nm were achieved in after 5 h at 70 °C but in 1 h at 90 °C. However, the photoluminescence intensity of these particles is about four times lower than that of the particles synthesized at 70 °C (Fig. S2†).

TEM images of Ag_2S–DMSA NIRQDs show mostly spherical and highly crystalline structure with particle sizes between 5 and 8 nm (Fig. 4a and b). The interplanar distance of the crystallite was measured to be 0.26 nm (Fig. 4c) which is correlated with the −121 plane of the monoclinic Ag_2S in the alpha phase (JCPDS: 14-0072).[36,37] Significant movement and aggregation were observed during the measurement possibly due to the presence of organic coating. Crystal sizes measured by TEM do not correlate well with the sizes calculated by the Brus equation, but sure are more reliable. Sizes obtained from TEM are slightly smaller than sizes measured by DLS as expected which is due to the presence of the coating material (Fig. S3†). Yet, sizes calculated by the Brus equation and reported in Tables 1 and 2 can be used to determine the influence of reaction variables on the particle size and hence the luminescence wavelength. Although the Brus equation is used frequently for size calculation of quantum dots, there are no reports in the literature where both the sizes measured by TEM and calculated by the Brus equation are presented for Ag_2S quantum dots. This is probably due to the significant differences in results as we observed here. None of the m_e and m_h values reported for Ag_2S provided diameters matching with those obtained from TEM. Recently, Zhang *et al.* reported size tunable synthesis of Ag_2S QDs through decomposition of Ag–diethyldithiocarbamate at high temperatures and measured sizes of QDs by TEM.[38] The smallest particles they have prepared have a broad luminescence centered at 975 nm with an average diameter of 2.4 nm. This is close to our largest particle diameter and luminescence peak. Yet, although not reported directly, from the available UV-absorbance data, it seems like their TEM based size analysis will not match to diameters calculated by the Brus equation either.

XPS analysis confirmed the chemical composition of the Ag_2S–DMSA NIRQDs. Binding energies (BE) and corresponding signals of Ag 3d and S 2p core levels are shown in Fig. 5. Ag has peaks at the BEs of 367.73 ($3d_{5/2}$) and 373.72 ($3d_{3/2}$) eV consistent with the +1 oxidation state in bulk Ag_2S.[39,40] The sulphur 2p region is fitted to two doublet sets; the intense pair ($2p_{3/2}$ at 163.39 eV) belongs to S of the coating material (DMSA). The weak pair ($2p_{3/2}$ at 161.51 eV) corresponds to the bond of Ag–S–Ag originating from the inorganic core.

DMSA coated Ag_2S QDs have a typical XRD pattern, as seen in Fig. 6. The bulk form of Ag_2S is in the alpha phase having the monoclinic crystal structure at room temperature.[37] However, Ag_2S QDs in nanoparticle form exhibit an amorphous pattern possibly due to the small size and organic coating around the inorganic core. Crystalline peaks are hidden under the amorphous peak. Annealing of QDs at 180 °C provided the typical XRD pattern matching with the monoclinic phase (JCPDS: 14-72).[15]

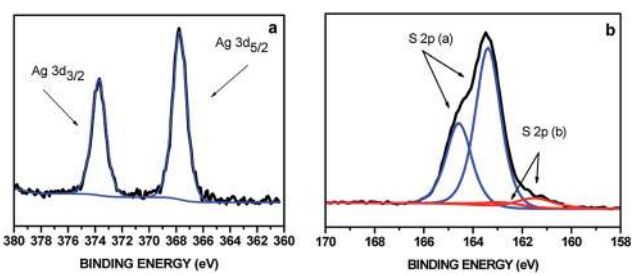

Fig. 5 XPS spectra of Ag_2S–DMSA NIRQDs: (a) Ag 3d region and (b) S 2p region.

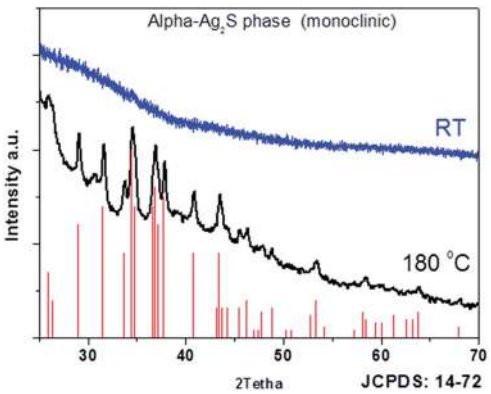

Fig. 6 XRD patterns of the Ag_2S–DMSA QDs as is (RT) and annealed at 180 °C.

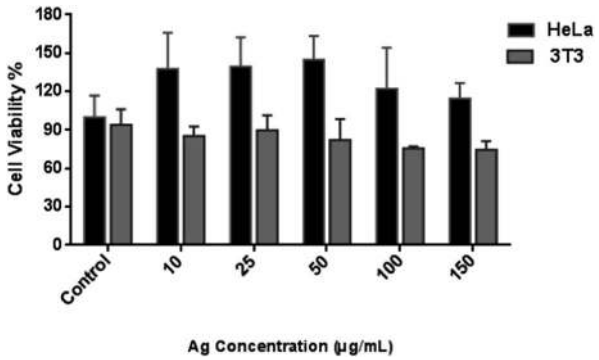

Fig. 7 Dose dependent cell viability of HeLa cancer cells and NIH/3T3 mouse fibroblast cells after 24 h incubation with Ag_2S–DMSA quantum dots.

Assessment of *in vitro* cytotoxicity

The toxicity of quantum dots is very critical for biological applications. Ag–chalcogenites were reported to exhibit almost no toxicity in different cancer cell lines.[14,21] In the case of BSA coated Ag_2S, cell proliferation was observed and this was attributed to BSA which may act as a nutrient.[41] We have shown the excellent biocompatibility of 2MPA coated Ag_2S not only in cancer cell lines but also in more susceptible NIH-3T3 cells.[20] Very recently, glutathione coated Ag_2S NIR QDs were reported to have negligible cytotoxicity in HepG2 and L929 cells.[22,42] Analysis of apoptosis and necrosis studies of Ag_2S coated with a multidentate polymer also indicated negligible cytotoxicity.[23]

The toxicity of DMSA coated Ag_2S quantum dots to HeLa and NIH-3T3 cells was evaluated using the MTT assay. In 24 h incubation, HeLa cells were not affected up to 150 µg mL^{-1} of Ag (corresponding to a QD concentration of 0.84 mg mL^{-1}) (Fig. 7). Similar to our previous results with Ag_2S–2MPA and the literature,[41] an increase in the cell viability, possibly indicating proliferation, was observed in HeLa cells. Causes of such behaviour are still not clear. NIH-3T3 fibroblast cells are more vulnerable than the cancer cell lines, and thus, the cell viability decreased by about 20% at 100 µg Ag per mL corresponding to 0.56 mg mL^{-1} incubation of the Ag_2S QDs which is an extremely high dose for these studies (Fig. 7). Most studies would stop at about 100 µg QD per mL dose. Overall, DMSA coated Ag_2S NIRQDs are cytocompatible nanoparticles.

Hemocompatibility assessment

Quantum dots' hemocompatibility was evaluated by studying hemolysis, the morphology of blood cells, complement activation (C3a), and coagulation activation, through the extrinsic and intrinsic pathways.

RBC integrity in the presence of QDs

The main cell population of the blood, erythrocytes, is the first to be evaluated in any hemocompatibility study.

Hemagglutination (erythrocyte aggregation), plasma membrane rupture or changes in cell morphology are amongst the possible reactions which can occur when a foreign nanomaterial is in contact with the whole blood. All these phenomena can induce severe circulatory disorders and even lethal toxicity. With a view to exclude any possible change in RBCs, we have characterized them by adopting complementary techniques. Following blood incubation with QDs, the hemolytic test was conducted according to the ASTM (Standard Practice for Assessment of Haemolytic Properties of Materials). The hemolysis rates determined in the presence of the formulations did not exceed 2% (see Table 3). Therefore these QDs

Table 3 Percentage of hemolysis, complement activation, and hemostasis activation (quick and TCA) after incubation at 37 °C of the QDs in whole blood

QDs (µg mL^{-1})	Hemolysis[a] (%)	Complement activation[b] (%)	Quick activation[c] (%)	TCA activation[c] (%)
1	0.08 ± 0.00	102.2 ± 6.6	93.4 ± 7.6	102.0 ± 5.2
10	0.22 ± 0.07	135.1 ± 6.3	98.4 ± 3.3	88.1 ± 6.1
100	0.22 ± 0.07	116.2 ± 1.1	100 ± 4.1	68.6 ± 4.5
Ctrl+	39.66 ± 0.07	158.9 ± 3.6	123.2 ± 3.2	—
Ctrl−	0.37 ± 0.09	100.0 ± 3.9	100 ± 4.3	100.6 ± 5.0

[a] Hemolysis percent represents free plasma hemoglobin released as a result of contact with the test material divided by the total blood hemoglobin multiplied by 100. Ctrl+: saponin, Ctrl−: PBS. [b] Complement activation is expressed as a % of C3a concentration, adopting normal blood incubated under the same conditions as 100%. Ctrl+: blood incubated with zymosan, Ctrl−: plasma with no additives. [c] Quick and TCA hemostasis assays are reported in % of the clotting ability of the sample compared to the clotting ability of a standard human plasma normalized to 100. Ctrl+: kaolin, Ctrl−: PBS.

may be considered non-hemolytic within the concentrations tested. This is in agreement with the hemolysis rates reported for BSA coated Ag_2S QDs at similar concentrations.[21] As a confirmation QDs under study did not affect the RBC size distribution profile and cell counts (Fig. 8). The microscopic analysis of blood smear (results not shown) also demonstrates the absence of any morphology changes after blood comes into contact with the samples. Therefore, we may conclude that these nanoparticles do not affect the integrity of erythrocytes, the major cellular component of blood. This observation is not really surprising taking into account that our QDs have a relatively strong negative zeta potential. These surface characteristics are therefore counteracting any possible ionic interaction with erythrocytes which have negative surface charges as well.[43]

Platelet and white blood cell (WBC) behavior in the presence of QDs

Platelets, the second main cell population of the blood, are by far more reactive to the presence of foreign surfaces compared to RBCs. Indeed one of their primary functions in hemostasis relies on their rapid adhesion to the foreign surface exposed by an injured vessel in order to limit any bleeding. The platelet plasma membrane is particularly rich in various biological receptors and is also well-known to interact with various synthetic surfaces, including those in the nano-size range.[44] As part of our immune system, some of our WBCs, in particular neutrophils and monocytes have to interact quickly with foreign materials in order to clear them from the blood compartment.

The comparison of the platelet and leucocyte size distribution of the blood control to the blood in contact with QDs (Fig. 8) clearly highlights that at the highest concentration of nanoparticles assessed, 100 μg mL^{-1}, no significant alteration is observed for any cell type. It is also the case for the global counting of these cells (results not shown). At a level of our pre-screening hemocompatibility study, these data therefore support the fact that Ag_2S–DMSA NIRQDs do not interact significantly with the various blood cell elements. This observation is of particular interest regarding platelets which are well-known to react when in contact with foreign body surfaces.

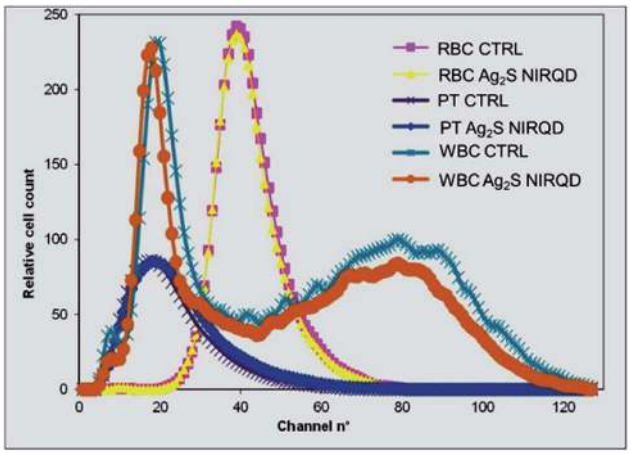

Fig. 8 Comparison of the blood cell distributions (red blood cells (RBCs), platelets (PTs) and white blood cells (WBCs) of the blood control to the blood incubated with Ag_2S NIRQDs (100 μg mL^{-1}).

The complement system is also part of our immune response to facilitate the elimination of certain pathogens from the body. But its chronic activation throughout the alternative pathway, *via* the nonspecific adsorption to foreign surface and cleavage of the C3 protein to produce C3a, can be responsible for hypersensitivity and anaphylaxis reactions.[45] Complement activation mediated by nanoparticles can also result in their rapid removal from systemic circulation by mononuclear cells *via* a receptor-mediated phagocytosis of complement. Based on the data provided in Table 3, only a slight activation of the complement system, which is not dose dependent in the range of QD concentrations tested, was detected.

Assessment of hemostasis in the presence of Ag_2S–DMSA QDs

The effect on hemostasis control was determined by coagulation assays, both through the extrinsic pathway (PT assay) and the intrinsic pathway (APTT assay). Clot formation was determined after blood incubation with QDs. The clotting ability of the standard plasma is assumed to be 100%. The longer it takes plasma to clot, the lower is its clotting ability, and the lower is the resulting test value expressed in percent to the standard plasma. It is also worth mentioning that these two coagulation pathways are intrinsically linked. For example, the tissue factor–factor VIIa complex initiating the extrinsic pathway is also capable of activation of factor IX of the intrinsic pathway; in turn, the intrinsic tenase complex influences the tissue factor-dependent pathway.[46] The extrinsic coagulation pathway was not affected by Ag_2S/DMSA NIRQDs, while the intrinsic pathway was significantly inhibited at the highest concentrations of the QDs (100 μg mL^{-1}) (Table 3). As reported recently, inhibition of intrinsic and extrinsic pathways of coagulation can be explained by the non-specific adsorption of proteins involved in the coagulation cascades onto the surface of materials involved.[47] Among these proteins, fibrinogen, factor IX, prothrombin, factor X, and antithrombin III deserve particular interest as key factors in the activation of all humoral blood reactions. The fact that the intrinsic pathway is specifically altered in contrast to the extrinsic mode is not really surprising keeping in mind that more protein factors are involved in the former one. Although it would be valuable to identify the exact nature of the factor(s) involved in the QD-mediated coagulation inhibition, this mechanistic study was outside of the main focus of our work.

In vitro cell imaging

The use of Ag_2S–DMSA NIRQDs as optical imaging agents was evaluated as well since such bio-applications are the major motivation behind such particles. A couple of examples found in the literature demonstrated *in vitro* imaging of cancer cells with Ag_2S NIRQDs emitting in the NIR-I[20] and NIR-II window.[12] Also, *in vivo* imaging of a nude mouse with Ag_2Se NIRQDs[14] and Ag_2S NIRQDs[17] has been recently reported. Here, HeLa cells incubated with Ag_2S–DMSA NIRQDs for 6 h were imaged under a fluorescence microscope. These QDs are easily excited at 532

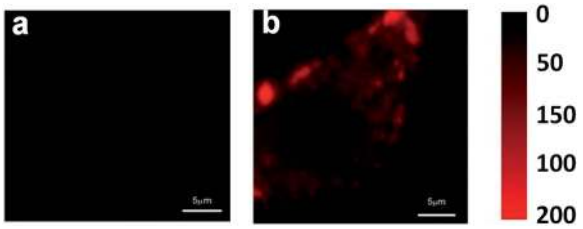

Fig. 9 Fluorescence image of HeLa cells (a) without and (b) with internalized Ag_2S–DMSA NIRQDs obtained using a confocal laser scanning microscope.

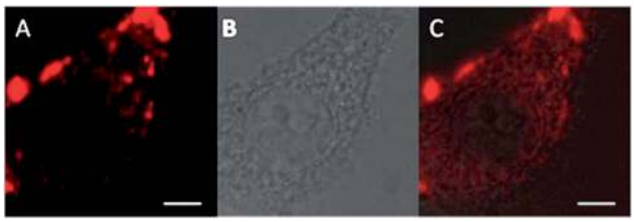

Fig. 10 Cellular uptake and localization of Ag_2S–DMSA NIRQDs by HeLa cells (150 μg mL^{-1} QDs, 6 h incubation). (A) Fluorescence, (B) transmission and (C) overlay channels of the confocal micrograph. Scale bar represents 5 μm.

nm which causes a minimal autofluorescence from the cells (Fig. 9a) but allows visualization of a very bright cellular image with a high intensity from QD internalized HeLa cells (Fig. 9b).

The confocal laser scanning microscopy image in Fig. 10 shows strong fluorescence of Ag_2S–DMSA NIRQDs in HeLa cells. These QDs have typical cytoplasmic distribution to endosomes and lysosomes with no nuclear uptake.

Conclusions

In vivo utilization of QDs as imaging agents and/or delivery vehicles requires a delicate balance of toxicity, biocompatibility, stability, luminescence quality, size and excitation/emission wavelengths. Considering all these requirements, Ag_2S NIRQDs present great potential. Utilization of DMSA, an FDA approved heavy metal chelating drug, as a coating and slow sulphur releasing agent under appropriate conditions (pH 7.5 and 70 °C and above) provided Ag_2S QDs with tunable emission between 730 and 900 nm with the best quality particles around the 800–860 nm range which is the desired window for medical purposes. The QY of these particles is as high as 6.5% and high enough for effective optical imaging. They are demonstrated as effective cytoplasmic imaging agents in HeLa cells. Recently, aqueous Ag_2S QDs coated with BSA were prepared with tunable sizes (within a range of 150 nm) in the second NIR region with the best particles emitting at around 1150 nm with 1.8% QY.[21] Considering the imaging devices and routine instrumentation, working in the second NIR window is difficult since it is beyond the limits of most widely used Si and PMT detectors.

DMSA coated Ag_2S NIRQDs showed good cytocompatibility and hemocompatibility in the *in vitro* experiments without any PEGylation or protein shell such as BSA. This achievement is significant and very valuable for *in vivo* experiments where a long blood circulation time and high level of cytocompatibility is necessary. These QDs do not affect the integrity of erythrocytes, do not interact with platelets and show only a slight alteration on the complement system and on the intrinsic pathway of coagulation. To the best of our knowledge this is the first report assessing the hemocompatibility of Ag_2S QDs in such detail. Drugs and targeting moieties can be conjugated to the surface carboxylates of these QDs. These NIR QDs hold great potential as new theranostic nanoparticles.

Acknowledgements

Ch. Sevrin has received the financial support of BioMiMedics, an Interreg Project. We would like to thank Dr Ugur Unal and Cansu Yildirim (KUYTAM, Koc University, Istanbul-Turkey) for XPS and XRD analyses and Dr Mehmet Ali Gulgun and Melike Yildizhan at SUNUM (Sabanci University, Istanbul-Turkey) for the TEM analysis.

Notes and references

1 R. Aswathy, Y. Yoshida, T. Maekawa and D. Kumar, *Anal. Bioanal. Chem.*, 2010, **397**, 1417–1435.
2 P. P. Ghoroghchian, M. J. Therien and D. A. Hammer, *Wiley Interdiscip. Rev.: Nanomed. Nanobiotechnol.*, 2009, **1**, 156–167.
3 H. Y. Chen, S. S. Cui, Z. Z. Tu, J. Z. Ji, J. Zhang and Y. Q. Gu, *Photochem. Photobiol.*, 2011, **87**, 72–81.
4 B. Blackman, D. Battaglia and X. Peng, *Chem. Mater.*, 2008, **20**, 4847–4853.
5 S. B. Rizvi, S. Ghaderi, M. Keshtgar and A. M. Seifalian, *Nano Reviews*, 2010, **1**, 5161.
6 A. Guchhait, A. K. Rath and A. J. Pal, *Sol. Energy Mater. Sol. Cells*, 2011, **95**, 651–656.
7 H. Ding, K.-T. Yong, W.-C. Law, I. Roy, R. Hu, F. Wu, W. Zhao, K. Huang, F. Erogbogbo, E. J. Bergey and P. N. Prasad, *Nanoscale*, 2011, **3**, 1813–1822.
8 N. Y. Morgan, S. English, W. Chen, V. Chernomordik, A. Russo, P. D. Smith and A. Gandjbakhche, *Acad. Radiol.*, 2005, **12**, 313–323.
9 Y. He, Y. Zhong, Y. Su, Y. Lu, Z. Jiang, F. Peng, T. Xu, S. Su, Q. Huang, C. Fan and S.-T. Lee, *Angew. Chem., Int. Ed.*, 2011, **50**, 5695–5698.
10 R. Xie, K. Chen, X. Chen and X. Peng, *Nano Res.*, 2008, **1**, 457–464.
11 G. Chen, F. Tian, Y. Zhang, Y. Zhang, C. Li and Q. Wang, *Adv. Funct. Mater.*, 2014, **24**, 2481–2488.
12 Y. Zhang, G. Hong, Y. Zhang, G. Chen, F. Li, H. Dai and Q. Wang, *ACS Nano*, 2012, **6**, 3695–3702.
13 Y. Du, B. Xu, T. Fu, M. Cai, F. Li, Y. Zhang and Q. Wang, *J. Am. Chem. Soc.*, 2010, **132**, 1470–1471.
14 Y.-P. Gu, R. Cui, Z.-L. Zhang, Z.-X. Xie and D.-W. Pang, *J. Am. Chem. Soc.*, 2011, **134**, 79–82.
15 P. Jiang, Z.-Q. Tian, C.-N. Zhu, Z.-L. Zhang and D.-W. Pang, *Chem. Mater.*, 2011, **24**, 3–5.

16 M. Yarema, S. Pichler, M. Sytnyk, R. Seyrkammer, R. T. Lechner, G. Fritz-Popovski, D. Jarzab, K. Szendrei, R. Resel, O. Korovyanko, M. A. Loi, O. Paris, G. n. Hesser and W. Heiss, *ACS Nano*, 2011, **5**, 3758–3765.
17 P. Jiang, C.-N. Zhu, Z.-L. Zhang, Z.-Q. Tian and D.-W. Pang, *Biomaterials*, 2012, **33**, 5130–5135.
18 K. P. Remya, T. Udayabhaskararao and T. Pradeep, *J. Phys. Chem. C*, 2012, **116**, 26019–26026.
19 G. A. Martínez-Castañón, M. G. Sánchez-Loredo, H. J. Dorantes, J. R. Martínez-Mendoza, G. Ortega-Zarzosa and F. Ruiz, *Mater. Lett.*, 2005, **59**, 529–534.
20 I. Hocaoglu, M. N. Cizmeciyan, R. Erdem, C. Ozen, A. Kurt, A. Sennaroglu and H. Y. Acar, *J. Mater. Chem.*, 2012, **22**, 14674–14681.
21 H. Y. Yang, Y. W. Zhao, Z. Y. Zhang, H. M. Xiong and S. N. Yu, *Nanotechnology*, 2013, **24**, 055706.
22 L. Tan, A. Wan and H. Li, *ACS Appl. Mater. Interfaces*, 2013, **6**, 18–23.
23 R. Gui, A. Wan, X. Liu, W. Yuan and H. Jin, *Nanoscale*, 2014, **6**, 5467–5473.
24 E. Sevinc, F. S. Ertas, G. Ulusoy, C. Ozen and H. Y. Acar, *J. Mater. Chem.*, 2012, **22**, 5137–5144.
25 W. Yantasee, K. Hongsirikarn, C. L. Warner, D. Choi, T. Sangvanich, M. B. Toloczko, M. G. Warner, G. E. Fryxell, R. S. Addleman and C. Timchalk, *Analyst*, 2008, **133**, 348–355.
26 J. H. Graziano, N. J. Lolacono, T. Moulton, M. Ellen Mitchell, V. Slavkovich and C. Zarate, *J. Pediatr.*, 1992, **120**, 133–139.
27 C. V. Durgadas, K. Sreenivasan and C. P. Sharma, *Biomaterials*, 2012, **33**, 6420–6429.
28 D. Painuly, A. Bhatt and V. K. Krishnan, *J. Biomater. Appl.*, 2014, **28**, 1125–1137.
29 C. V. Durgadas, C. P. Sharma and K. Sreenivasan, *Nanoscale*, 2011, **3**, 4780–4787.
30 L. E. Brus, *J. Chem. Phys.*, 1984, **80**, 4403–4409.
31 L. Brus, *J. Phys. Chem.*, 1986, **90**, 2555–2560.
32 S. H. Ehrlich, *J. Imaging Sci. Technol.*, 1993, **37**, 73–91.
33 A Guide to Recording Fluorescence Quantum Yields, http://www.horiba.com/fileadmin/uploads/Scientific/Documents/Fluorescence/quantumyieldstrad.pdf.
34 S. Celebi, A. K. Erdamar, A. Sennaroglu, A. Kurt and H. Y. Acar, *J. Phys. Chem. B*, 2007, **111**, 12668–12675.
35 W. Y. S. Hui Li and W.-H. Shih*, *Ind. Eng. Chem. Res.*, 2007, **46**, 2013–2019.
36 H. E. Swanson, J. H. deGroot, E. H. Evans, M. I. Cook and S. United, *Standard X-Ray diffraction powder patterns*, National Bureau of Standards, Washington D.C., 1960.
37 O. Madelung, *Semiconductors: Data Handbook*, Springer-Verlag Berlin Heidelberg, New York, 3rd edn, 2004, p. 1528.
38 Y. Zhang, Y. Liu, C. Li, X. Chen and Q. Wang, *J. Phys. Chem. C*, 2014, **118**, 4918–4923.
39 Handbook of the Elements and Native Oxides, http://www.xpsdata.com/XI_BE_Lookup_table.pdf.
40 R. B. C. Orléans, http://www.lasurface.com/database/elementxps.php.
41 R. Xing, S. Liu and S. Tian, *J. Nanopart. Res.*, 2011, 4847–4854, DOI: 10.1007/s11051-011-0462-4.
42 Y. Zhao and Z. Song, *Mater. Lett.*, 2014, **126**, 78–80.
43 C. Grandfils, P. Foresto, B. Riquelme, J. Valverde and D. Sondag-Thull, *J. Biomed. Mater. Res., Part A*, 2008, **84A**, 535–544.
44 A. Radomski, P. Jurasz, D. Alonso-Escolano, M. Drews, M. Morandi, T. Malinski and M. W. Radomski, *Br. J. Pharmacol.*, 2005, **146**, 882–893.
45 D. S. R. Paul M Knopf, S.-H. Hai, J. McMurry, W. Martin and A. S. De Groot, *Immunol. Cell Biol.*, 2008, **86**, 4.
46 M. B. Gorbet and M. V. Sefton, *Biomaterials*, 2004, **25**, 5681–5703.
47 B. I. Cerda-Cristerna, H. Flores, A. Pozos-Guillén, E. Pérez, C. Sevrin and C. Grandfils, *J. Controlled Release*, 2011, **153**, 269–277.